PHYSICAL REVIEW C **84**, 011601(R) (2011)

Synthesis of $N = 127$ isotones through (p,n) charge-exchange reactions induced by relativistic ^{208}Pb projectiles

A. I. Morales,[1,*] J. Benlliure,[1] J. Agramunt,[2] A. Algora,[2,3] N. Alkhomashi,[4,†] H. Álvarez-Pol,[1] P. Boutachkov,[5] A. M. Bruce,[6] L. S. Cáceres,[5] E. Casarejos,[1,‡] A. M. Denis Bacelar,[6] P. Doornenbal,[5] D. Dragosavac,[1] G. Farrelly,[4] A. Gadea,[7,§] W. Gelletly,[4] J. Gerl,[5] M. Górska,[5] J. Grebosz,[5] I. Kojouharov,[5] F. Molina,[2] D. Pérez-Loureiro,[1] S. Pietri,[4,‖] Z. Podolyák,[4] P. H. Regan,[4] B. Rubio,[2] H. Shaffner,[5] S. J. Steer,[4] S. Tashenov,[5] S. Verma,[1,¶] and H. J. Wollersheim[5]

[1]*Universidade de Santiago de Compostela, 15782 Santiago de Compostela, Spain*

[2]*IFIC, CSIC-Universidad de Valencia, E-46071 Valencia, Spain*

[3]*Institute of Nuclear Research of the Hungarian Academy of Sciences, H-4001 Debrecen, Hungary*

[4]*Department of Physics, University of Surrey, Guildford GU2 7XH, United Kingdom*

[5]*GSI, Planckstrasse 1, D-64291 Darmstadt, Germany*

[6]*School of Computing, Engineering and Mathematics, University of Brighton, Brighton BN2 4GJ, United Kingdom*

[7]*INFN-Laboratori Nazionali di Legnaro, I-35020 Legnaro, Italy*

(Received 12 March 2011; published 20 July 2011)

The production cross sections of four $N = 127$ isotones (^{207}Hg, ^{206}Au, ^{205}Pt, and ^{204}Ir) have been measured using (p,n) charge-exchange reactions, induced in collisions of a ^{208}Pb primary beam at 1 A GeV with a Be target. These data allow one to investigate the use of a reaction mechanism to extend the limits of the chart of nuclides toward the important r-process nuclei in the region of the third peak of elemental abundance distribution.

DOI: 10.1103/PhysRevC.84.011601 PACS number(s): 25.70.Mn, 25.70.Kk, 27.80.+w, 29.38.Db

The production of nuclei beyond the current limits of experimental synthesis is one of the foremost subjects for nuclear physicists, providing peerless opportunities to investigate not only the properties of exotic nuclei at extreme conditions of temperature, angular momentum, and isospin but also the nuclear reactions that occur in the astrophysical processes that lead to the formation of the heaviest elements in the universe [1]. These issues will be approached in the next generation of in-flight radioactive-beam facilities [2–4], where many of the remote exotic nuclei will be accessible for the first time.

In recent decades, fragmentation and fission reactions have proved to be useful means for the production of neutron-rich nuclei throughout the nuclear chart. Light neutron-rich nuclei have been synthesized using the fragmentation of ^{48}Ca [5], whereas the fission reactions have been satisfactorily used to produce medium-mass neutron-rich nuclei [6–8]. The fragmentation of secondary beams of neutron-rich fission products, such as ^{132}Sn, has also been proposed to produce extremely neutron-rich nuclei [9]. The challenge of obtaining access to the heavy neutron-rich nuclei has been tackled recently using the fragmentation of heavy stable projectiles such as ^{208}Pb or ^{238}U at relativistic energies [10,11]. It is particularly difficult to reach the neutron-rich region "south" of lead, where only a few nuclei approaching the β stability line have been synthesized to date.

The exploration of the nuclear chart in the neutron-rich region around $N = 126$ will shed more light on the evolution of shell closures in heavy many-body systems. It has been shown that the robustness of the $N = 20$ and $N = 28$ shells weakens with the neutron excess [12,13]. There are also indications of the weakening of the $N = 50$ shell gap as the proton number decreases [14,15]. In the case of the $N = 82$ closed shell, the appearance of the shell-quenching phenomenon for neutron-drip-line nuclei is still being debated [16–18]. The exploration of the neutron-rich $N = 126$ isotones is also important for the modeling of the r-process in the region of the third peak of the elemental abundance distribution. Indeed, the properties of nuclei at the $A \approx 195$ waiting point determine the flow of matter to heavier fissioning r-process nuclei [19].

Hitherto, attempts to synthesize the challenging $N = 126$ neutron-rich nuclei were centered on the fragmentation of ^{208}Pb and ^{238}U. The fragmentation mechanism is characterized by large fluctuations in the neutron-to-proton ratio and the excitation energy of the projectile residue. Extremely neutron-rich nuclei can be produced through the cold fragmentation channel, in which the incident projectile mainly loses protons during the abrasion stage and the excitation energy of the prefragment is below the neutron separation energy.

We propose here an alternative reaction mechanism to explore the interesting neutron-rich region around $N = 126$, taking advantage of (p,n) charge-exchange reactions of relativistic ^{208}Pb projectiles. Thus far, our experimental knowledge of charge exchange at relativistic energies has been focused mostly on (n,p) charge exchange of intermediate- [20] and heavy-mass nuclei [21,22].

The charge-exchange reactions involving heavy relativistic projectiles are described as peripheral nuclear collisions [23]

*anaisabel.morales@usc.es

†Present address: KACST, P.O. Box 6086, Riyadh 11442, Saudi Arabia.

‡Present address: Universidade de Vigo, E-36310 Vigo, Spain.

§Present address: IFIC, CSIC-Universidad de Valencia, E-46071 Valencia, Spain.

‖Present address: GSI, Planckstrasse 1, D-64291 Darmstadt, Germany.

¶Present address: University of Delhi, Delhi 110007, India.

between the projectile and target in a participant-spectator context [20]. Two-body nucleon-nucleon interactions induce the charge exchange between the projectile and target nuclei. There are two charge-exchange mechanisms [24] responsible for the modification of the nuclear charge. The first is a quasielastic isospin-exchange collision between a projectile nucleon n_p and a target nucleon n_t, where n_p receives the total kinetic energy of n_t ending up in the phase volume of the projectile prefragment, with the exchange of a virtual $\pi^{\pm}$ or $\rho^{\pm}$ meson; the second is an inelastic isospin-exchange collision where a nucleon from either the target or the projectile is excited into the $\Delta(1232)$-resonance state by the exchange of a virtual pion between both nuclei. Subsequently, the Δ resonance decays, emitting a real pion. Only when the emitted pion is charged and escapes from the nucleus will the charge exchange be effective. It was shown that the contribution of these two mechanisms can be observed in the velocity distributions of the charge-exchange products [22].

In this work we provide a systematic comparison of the ^{208}Pb single (p,n) charge-exchange cross sections of ^{207}Hg, ^{206}Au, ^{205}Pt, and ^{204}Ir with the simulated fragmentation yields of the same isotopes using ^{238}U projectiles. The data reveal an approach to studying the primary structure of the neutron-rich $N = 126$ isotones from the β decay of the mother $N = 127$ nuclei, produced in (p,n) charge-exchange reactions of relativistic ^{208}Pb projectiles.

The heavy neutron-rich nuclei were produced at GSI Darmstadt through (p,n) charge-exchange reactions between a ^{208}Pb projectile at 1 A GeV and a Be target 1.6 g/cm^2 thick. The SIS-18 synchrotron delivered the primary beam with a repetition cycle of 10 s and a spill length of 2 s, with intensities of up to 10^9 ions/spill. The reaction products were analyzed with the magnetic spectrometer fragment separator (FRS) [25], specifically tuned to transmit ^{206}Au along the central trajectory. The FRS is a high-resolution forward spectrometer with a momentum-resolving power of 1500 for an emittance of 20π mm mrad, a momentum acceptance of 1.5%, and an angular acceptance around its central trajectory of 15 mrad. The spectrometer is divided into two symmetrical stages in order to preserve the achromatism of the system. In the first section, the residues are selected according to their mass-over-charge ratio A/Q, with a resolution given by the dispersion of their magnetic rigidity $B\rho$ and the acceptance of the spectrometer. A profiled Al degrader is placed at the intermediate image plane to separate the transmitted nuclei with an additional bend that depends on the ratio of the magnetic rigidities in the first and second sections of the separator [26].

The nuclei traversing the FRS were identified according to their mass-over-charge ratio A/Q and their atomic charge Q. The former was determined from the magnetic rigidity and the velocity of the fragments, whereas the latter was deduced from the energy loss registered in two multisampling ionization chambers (MUSIC) located at the final image plane of the spectrometer. The magnetic rigidity was obtained from the positions of the fragments at the intermediate and final image planes, measured using two plastic scintillators that also provided the time of arrival of the fragments at both focal planes and then their velocity.

The relativistic energies employed in the current experiment favored that the equilibrium charge state of the fragmentation residues produced in the target was nearly fully stripped. However, because of the large atomic numbers of the selected nuclei, their probability of ionization in their interaction with the optical elements and detectors present in the FRS was enhanced. The charge-state equilibrium close to fully ionized nuclei was restored by using three stripping Niobium foils: the first behind the target (220 mg/cm^2), the second behind the energy degrader at the intermediate image plane of the separator (105 mg/cm^2), and the third in between the two MUSIC chambers (230 mg/cm^2).

In spite of the high electronic affinity of the Niobium, a small percentage of the reaction residues remained in their hydrogen-like charge state in the first and second sections of the FRS, as well as in the MUSIC chambers. Their presence hence affected the identification of the nuclei of interest in A/Q, with the FRS, and in atomic number, with the MUSIC chambers. In particular, $(A-3, Z)$ residues with a hydrogen-like ionic charge state $(Q = Z - 1)$ have a similar magnetic rigidity as fully stripped (A, Z) nuclei. Since the neutron-rich $(A-3, Z)$ fragments typically have production cross sections around two orders of magnitude larger than the cross sections of the isotopes with three more neutrons (A, Z), a few percent of the production of $(A-3, Z)$ fragments with a hydrogen-like ionic charge state could represent almost 100% contamination in (A, Z) fully stripped nuclei. Moreover, the ionic charge changes within the gas of the ionization chambers contributed to degrade the energy resolution achieved with these detectors.

In order to approach this challenge, the atomic charge-state changes of the nuclei traversing the FRS were determined by measuring the difference in magnetic rigidity in the intermediate degrader, quantified according to the variable $\Delta E_{\mathrm{deg}} = (\gamma_1 - \gamma_2) u A/Q$, with γ being the relativistic factor in the first (1) and second (2) sections of the FRS, A being the mass number of the ion, and u being the atomic mass unit. Also, the ionic charge changes occurring in the stripping Niobium foil placed between the two MUSIC chambers were identified by comparing the energy losses registered by the two MUSICs. In this case, the fully stripped ions correspond to the maximum energy loss signal $\mathrm{Q}^{\mathrm{max}}$ measured by any of the two chambers. A detailed description of the method can be found in Ref. [27].

Figure 1 shows the two-dimensional cluster plot of the variables ΔE_{deg} and $\mathrm{Q}^{\mathrm{max}}$ for a FRS magnetic setting centered on ^{206}Au. In Fig. 1, the four lines indicate events compatible with four ionic charges inside the FRS. The dotted line, labeled (1e-0e), corresponds to fragments leaving the target as hydrogen-like ions and losing the electron at the intermediate degrader. The dashed line labeled (0e-1e) represents nuclei leaving the target fully stripped but gaining one electron in the energy degrader at the intermediate image plane. The solid line labeled (0e-0e) corresponds to fully stripped nuclei in both sections of the FRS. Finally, the dashed-dotted line labeled (1e-1e) indicates nuclei leaving the target with one electron and keeping this electron all along the FRS.

The excellent magnetic resolution of the spectrometer allows the separation of the different charge states, even between the (0e-0e) and (1e-1e) contributions to a large extent,

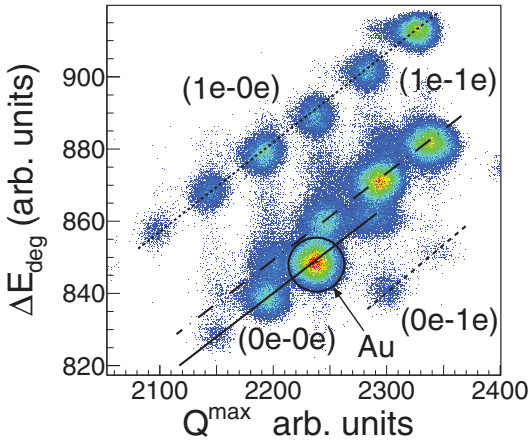

FIG. 1. (Color online) Correlation plot of the effective energy loss in the intermediate degrader and the atomic charge for a FRS magnetic setting centered on ^{206}Au. Each labeled set of clusters corresponds to a different charge-state configuration.

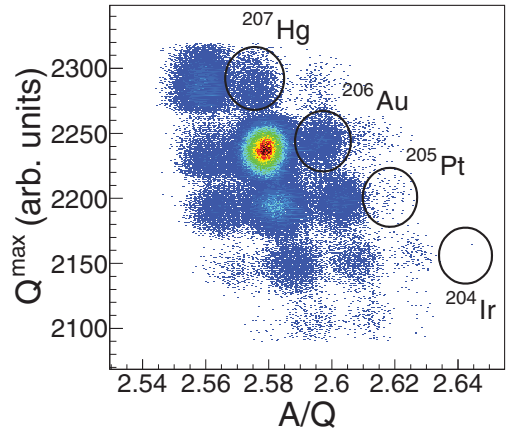

FIG. 2. (Color online) Two-dimensional cluster plot of the atomic charge as a function of the A/Q ratio.

as Fig. 1 illustrates. The only misidentifications may be given by two contributions: first, the $(A-3, Z)$ nuclei that acquire one electron in the target, conserve it along the FRS, and lose it at the exit of the FRS or in the stripper foil between both MUSIC chambers and, second, the $(A, Z+1)$ nuclei that gain one electron at the target and keep it in their flight through the FRS and the two MUSIC chambers. Fortunately, the probability for these combinations is rather low, producing a moderate contamination, as explained below and shown in Table I.

The mass identification matrix of the A/Q ratio as a function of the atomic charge $Q^{\max}$ for fully stripped nuclei is shown in Fig. 2. The $N = 127$ isotones produced through (p,n) charge-exchange reactions are labeled in Fig. 2. The high mass resolution obtained after applying the identification procedure allows one to determine the production cross sections of the transmitted nuclei with high accuracy. The small amount of contamination still present in the (0e-0e) distribution can be inferred from the clusters of dots appearing on the right side of ^{207}Hg and ^{206}Au in Fig. 2. Their A/Q and $Q^{\max}$ values correspond to those of ^{208}Hg and ^{207}Au, but their yields can only be understood as being due to the hydrogen-like contaminants traversing the FRS (which are ^{205}Hg for ^{208}Hg and ^{204}Au and ^{207}Hg for ^{206}Au).

The expected rates of each contaminant nucleus are calculated as the product between its fragmentation yields and the survival probability of the corresponding charge-state configuration along the beam line. In this work, the code GLOBAL [28] has been used to calculate the production probabilities of the charge-state contaminants after the target, the intermediate and final image planes, and the two MUSIC chambers. Finally, the percentage of contamination introduced by these hydrogen-like nuclei in the cross sections of the $N = 127$ isotones is determined as the ratio between the expected production of contaminants and the yields of the $N = 127$ nuclei. Table I summarizes the charge-state contaminants for each $N = 127$ isotone, followed by the percentage of contamination in the measured cross sections in parentheses. For proton numbers over 78, the production rates of $N = 127$ isotones exceed by far the yields of hydrogen-like contaminants, thus confirming unambiguously their production through (p,n) charge-exchange reactions.

TABLE I. Single (p,n) charge-exchange cross sections and charge-state contaminants (percentages are given in parentheses).

Nucleus	σ (mb)	Contaminants
^{207}Hg	$0.11(5)10^{-1}$	^{207}Tl (3%), ^{204}Hg (1%)
^{206}Au	$0.36(12)10^{-3}$	^{206}Hg (3.5%), ^{203}Au (2%)
^{205}Pt	$0.57(18)10^{-5}$	^{205}Au (12%), ^{202}Pt (5%)
^{204}Ir	$0.19(16)10^{-6}$	^{204}Pt (13%), ^{201}Ir (26%)

The production rates of the nuclear species investigated were obtained by measuring the number of ions transmitted to the final image plane of the FRS. The production cross sections were determined after correcting these yields for losses due to beam attenuation and secondary reactions in the different materials placed throughout the FRS for losses due to the rejection of the charge states in the data analysis and for losses due to an incomplete transmission of the ions in the image planes. The measured yields were normalized to the fragmentation cross section of ^{202}Ir, measured in a previous experiment under analogous conditions [10], in order to account for the total number of incident projectiles and the dead time of the data acquisition system. The corrections for beam attenuation, secondary nuclear reactions, and charge states were calculated for each nuclear species using the codes KAROL [29] and GLOBAL [28], whereas the transmission correction was applied to the residues partially transmitted in one or both focal planes. The uncertainties in beam attenuation and secondary reactions amount to 10% [29], and the uncertainties associated with the correction for incompletely stripped ions and transmission amount to 5% and 20%, respectively [27].

Table I summarizes the charge-exchange cross sections of the $N = 127$ isotones. The uncertainties associated with these measurements include the statistical and the systematic effects. The systematic uncertainties embody the errors related to the yield corrections and the reference cross section.

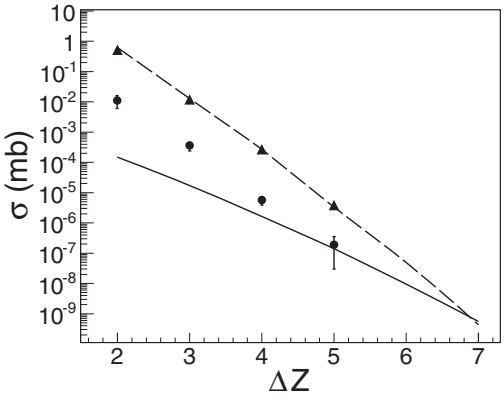

FIG. 3. Production cross sections of charge-exchange $N = 127$ isotones (dots, this work) and $N = 126$ fragmentation residues (triangles, from Ref. [10]) as a function of the number of protons removed from the projectile ^{208}Pb. The lines represent fragmentation cross sections of $N = 127$ (solid line) and $N = 126$ (dashed line) isotones obtained with the COFRA [30] code for reactions induced by ^{238}U and ^{208}Pb projectiles, respectively.

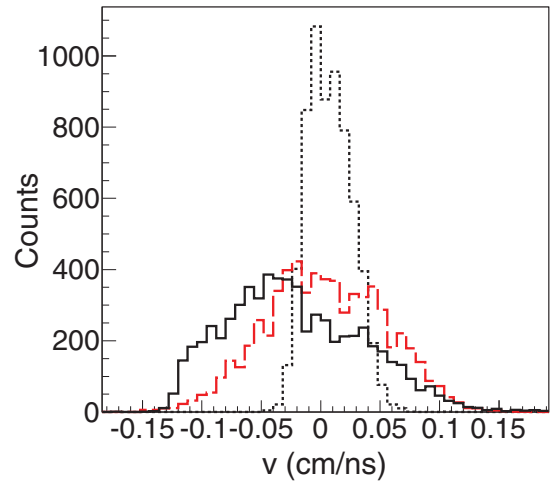

FIG. 4. (Color online) Longitudinal velocity distributions of ^{205}Au (dashed line) and ^{206}Au (solid line) fragments and of the beam nuclei ^{208}Pb (dotted line) in the reference frame of the latter.

Figure 3 shows the evolution of the measured charge-exchange cross sections for the four $N = 127$ isotones (dots) as a function of the number of protons removed from the primary beam, ^{208}Pb. Figure 3 also shows the cross sections of the analogous $N = 126$ isotones (triangles) synthesized by cold fragmentation of ^{208}Pb [10]. The cross sections of the $N = 127$ nuclei produced by fragmentation of ^{238}U have been simulated with the code COFRA [30] (solid line) for comparison. We have also simulated the fragmentation cross sections of the $N = 126$ isotones from ^{208}Pb beams (dashed line). In this last case, the perfect agreement with the measured data illustrates the predictive power of this code.

Looking in detail, one can observe that the production yields of the $N = 127$ isotones show the same slope as the cross sections of the $N = 126$ isotones. This indicates that the proton removal channels dominate the trend followed by the measured charge-exchange cross sections. Indeed, the constant ratio between the measured charge-exchange yields and the fragmentation yields of the analogous proton removal channel is expected since the charge-exchange mechanism takes place in peripheral nuclear collisions between projectile and target and, in the case of the inelastic channel, the isospin exchange can be only detected if the pion escapes from the nuclear surface, which is less likely to occur than the abrasion of a proton.

We also learn from Fig. 3 that the (p,n) charge exchange of lead beams is the optimal mechanism to produce the $N = 127$ isotones with a proton number larger than or equal to 78, whereas for lower Z the fragmentation of ^{238}U (solid line) is more adequate.

In order to get a better understanding of the (p,n) charge-exchange mechanism, the velocity distributions for ^{205}Au and ^{206}Au are shown in Fig. 4. These two reaction products were produced in the collision ^{208}Pb + ^{9}Be at 1 A GeV. While the residue ^{205}Au was most commonly produced by the removal of three protons, the nucleus ^{206}Au was unequivocally synthesized through a (p,n) charge-exchange interaction plus the removal of two protons. Figure 4 also shows the velocity of the lead projectile to illustrate the contribution of the momentum dispersion and the energy straggling of the fragment separator to the measured velocities. These observables were obtained from the magnetic rigidity $B\rho$ of the nuclei in the intermediate image plane and were further transformed into the reference frame of the projectile nucleus in the center of the target by Lorentz transformation. The transformed velocities were corrected by the energy loss of the projectile in the first half of the target and the energy loss of the residue in the second half of the target and the first stripping Nb foil. The momentum resolution is then given by the resolution in $B\rho$, $\Delta B\rho/B\rho \approx 5 \times 10^{-4}$, which improves the time-of-flight resolution by one order of magnitude.

The longitudinal velocities of the fragmentation residues decrease as the number of protons removed from the projectile increases [30]. Looking at Fig. 4, the velocity distribution of the three-proton removal product ^{205}Au is closer to the projectile velocity than the distribution of the two-proton removal and one (p,n) charge-exchange residue ^{206}Au. The lower velocities in the charge-exchange nucleus ^{206}Au can be explained as being due to the excitation of the Δ resonance in the inelastic charge-exchange channel. In this case, the velocity of the reaction products is reduced because of the mean energy transferred to the pion, by approximately 300 MeV.

Under the present experimental conditions, the energy shift induced by the excitation of the Δ-resonance state and the subsequent emission of the pion corresponds to an average velocity shift of approximately 0.03 cm/ns. Although the thickness of the target used in this work prevents an accurate unfolding of the measured distributions as performed in Ref. [22], the distribution of ^{206}Au shows a clear structure at smaller velocities in the range compatible with the shift induced by the inelastic charge-exchange channel. The appearance of this slower component in the velocity distribution of ^{206}Au can then be considered as a clear sign pointing

to charge exchange as the production mechanism for the $N = 127$ nuclei.

Four $N = 127$ isotones have been synthesized unequivocally in (p,n) charge-exchange collisions in the reaction ^{208}Pb + ^{9}Be at 1 A GeV. The lower velocities of those nuclei compared to others produced in pure nucleon removal collisions indicate a considerable role of the inelastic charge-exchange channel through the excitation of the Δ resonance. Given a systematic comparison, the measured charge-exchange cross sections of ^{208}Pb exceed the simulated fragmentation cross sections of ^{238}U for the $A = 205 \rightarrow 207$, $N = 127$ isotones. For lower-mass isotones, the fragmentation of ^{238}U results in a more appropriate production mechanism.

Summarizing, this work represents a step further in the attempts to expand the chart of nuclides toward the neutron drip line in the region around $N = 126$. Indeed, charge exchange has proved to be an optimum reaction mechanism to produce neutron-rich nuclei "south" of lead, of particular importance not only for investigating the evolution of shell closures in heavy nuclear systems but also for understanding the r-process stellar nucleosynthesis.

This work was supported by the Spanish MICINN under Grants No. FPA2007-62652, No. FPA2008-6419-C02-01, and No. FPU-AP2007-04543 and by the program "Ingenio 2010, Consolider CPAN," the Galician Regional Government under "Unidades Competitivas 2010/57," the EP-SRC/STFC(UK), AWE plc.(UK), the EU Access to Large Scale Facilities Programme (Eurons, EU Contract No. 506065), the German BMBF, the Hungarian Science Foundation, and the Italian INFN.

[1] E. M. Burbidge *et al.*, Rev. Mod. Phys. **29**, 547 (1957).
[2] [http://www.rarf.riken.go.jp/Eng/facilities/RIBF.html].
[3] [http://www.gsi.de/fair].
[4] [http://www.frib.msu.edu].
[5] M. Mocko *et al.*, Phys. Rev. C **74**, 054612 (2006).
[6] M. Bernas *et al.*, Phys. Lett. B **331**, 19 (1994).
[7] P. Armbruster *et al.*, Phys. Rev. Lett. **93**, 212701 (2004).
[8] T. Ohnishi *et al.*, J. Phys. Soc. Jpn. **79**, 073201 (2010).
[9] K. Helariutta *et al.*, Eur. Phys. J. A **17**, 181 (2003).
[10] T. Kurtukian, in Proceedings of the IX International Workshop "Nuclei in the Cosmos", CERN, Geneva, Switzerland, 2006, PoS(NIC-IX)008.
[11] H. Alvarez-Pol *et al.*, Phys. Rev. C **82**, 041602 (2010).
[12] T. Motobayashi *et al.*, Phys. Lett. B **346**, 9 (1995).
[13] H. Scheit *et al.*, Phys. Rev. Lett. **77**, 3967 (1996).
[14] A. Prevost *et al.*, Eur. Phys. J. A **22**, 391 (2004).
[15] T. Rzkaca-Urban *et al.*, Phys. Rev. C **76**, 027302 (2007).
[16] T. Kautzsch *et al.*, Eur. Phys. J. A **9**, 201 (2000).
[17] I. Dillmann *et al.*, Phys. Rev. Lett. **91**, 162503 (2003).
[18] A. Jungclaus *et al.*, Phys. Rev. Lett. **99**, 132501 (2007).
[19] J. J. Cowan *et al.*, Phys. Rep. **208**, 267 (1991).
[20] K. Sümmerer *et al.*, Phys. Rev. C **52**, 1106 (1995).
[21] C. A. Bertulani *et al.*, Nucl. Phys. A **674**, 527 (2000).
[22] A. Kelić *et al.*, Phys. Rev. C **70**, 064608 (2004).
[23] C. A. Bertulani, Nucl. Phys. A **554**, 493 (1993).
[24] C. Gaarde, Annu. Rev. Nucl. Part. Sci. **41**, 187 (1991).
[25] H. Geissel *et al.*, Nucl. Instrum. Methods Phys. Res. B **70**, 286 (1992).
[26] K.-H. Schmidt *et al.*, Nucl. Instrum. Methods Phys. Res. A **260**, 287 (1987).
[27] E. Casarejos *et al.*, Phys. Rev. C **74**, 044612 (2006).
[28] C. Scheidenberger *et al.*, Nucl. Instrum. Methods Phys. Res. B **142**, 441 (1998).
[29] P. J. Karol, Phys. Rev. C **11**, 1203 (1975).
[30] J. Benlliure *et al.*, Nucl. Phys. A **660**, 87 (1999).